

Journal of
**Micro/Nanolithography,
MEMS, and MOEMS**

SPIEDigitalLibrary.org/jm3

**Improvement of insertion loss and
quality factor of flexural plate-wave-
based alpha-fetoprotein biosensor using
groove-type reflective grating structures**

Chang-Yu Lin
I-Yu Huang
Je-Wei Lan



SPIE

Improvement of insertion loss and quality factor of flexural plate-wave-based alpha-fetoprotein biosensor using groove-type reflective grating structures

Chang-Yu Lin

I-Yu Huang

Je-Wei Lan

National Sun Yat-Sen University
Department of Electrical Engineering
70, Lien-Hai Road
Kaohsiung 80424, Taiwan
E-mail: iyuhuang@mail.nsysu.edu.tw

Abstract. Conventional flexural plate-wave (FPW) transducers have limited applications in biomedical sensing due to their disadvantages such as high insertion loss and low quality factor. To overcome these shortcomings, we propose a FPW transducer on a low phase velocity insulator membrane (5- μm -thick SiO_2) with a novel groove-type reflective grating structure design. Additionally, a cystamine self-assembly monolayer and a glutaraldehyde cross-linking layer are implemented on the backside of the FPW device to immobilize alpha-fetoprotein (AFP) antibody. A FPW-based AFP biosensor with low detection limit (5 ng/mL) can be achieved and used to measure the extreme low concentration of AFP antigen in human serum for early detection of hepatocellular carcinoma. The proposed FPW-based AFP biosensor also demonstrates a very high quality factor (206), low insertion loss (-40.854 dB), low operating frequency (6.388 MHz), and high sensing linearity (90.7%). © The Authors. Published by SPIE under a Creative Commons Attribution 3.0 Unported License. Distribution or reproduction of this work in whole or in part requires full attribution of the original publication, including its DOI. [DOI: [10.1117/1.JMM.12.1.013017](https://doi.org/10.1117/1.JMM.12.1.013017)]

Subject terms: flexural plate-wave; insertion loss; quality factor; groove-type reflective grating structures; self-assembly monolayer; alpha-fetoprotein biosensor.

Paper 12131 received Dec. 17, 2012; revised manuscript received Feb. 24, 2013; accepted for publication Mar. 1, 2013; published online Mar. 20, 2013.

1 Introduction

Over the past few decades, many tumor markers have been proposed as important indicators to screen cancer patients in clinical applications. For instance, discovered by Bergstrand and Czar,^{1,2} alpha-fetoprotein (AFP) is one among the important tumor markers produced by embryonic hepatic cells and the yolk sac.³ Typically, the serum AFP level in a healthy adult is lower than 20 ng/mL. The high concentrations of AFP in adult have been discovered in hepatocellular carcinoma (HCC) and malignant germ cell tumors of the ovary and testis.⁴ In Taiwan and other Asian countries, AFP is commonly used as a tumor marker to screen HCC.

Although the conventional immunoassay methods such as radioimmunoassay and non-isotopic immunoassays [e.g., enzyme-linked immunosorbent assay (ELISA)] both have the advantages of very low detection limit (<10 ng/mL) and accuracy ($>90\%$), they are time-consuming and require skilled personnel to operate in a laboratory.^{5,6} Recently, due to an increasing need for rapid immunoassay test kits for clinical applications, many miniaturized immunosensors with high mass-sensitivities have been developed by various physical transducers to reduce the response time, testing cost, and skilled operation requirement. Combined with the essential specificity of antigen-antibody reactions, some of these immunosensors have gained attention as methods for clinical diagnosis.^{7–19}

In general, the performance of an immunosensor is measured by its capability to detect molecular layers deposited on a surface. For instance, the loading mass on the sensing surface of conventional acoustic sensors can affect those propagating properties of the acoustic wave. Among the

acoustic sensors, Lamb waves-based acoustic sensors are frequently used because of their high sensitivity to mass-loading. One of these Lamb modes, the zero order anti-symmetrical mode (A_0), also called flexural plate-wave (FPW), is very suitable for biosensing applications because it has low phase velocity and small radiation loss when propagated in the testing liquid. FPW-based acoustic biosensors have many clinical, industrial, environmental, and biological sensing applications as they demonstrate high sensitivity and accuracy, short response time, low cost, and operating frequency. Any small changes in the mass of floating thin plate of the FPW transducer resulting in a change of the acoustic wave velocity can be measured indirectly as a change in center frequency of the FPW-based biosensor.^{9–19} However, the high insertion loss and low quality factor of conventional FPW-based biosensors have limited their applications. To enhance the quality factor and reduce the insertion loss and phase velocity of a FPW-based biosensor, this paper introduces a novel groove-type reflective grating structure (RGS) and adopts a low phase velocity insulator membrane (5- μm -thick SiO_2) to replace the conventional silicon-based membrane.

The highly specific AFP antigen-antibody interaction is a good candidate for the AFP molecular recognition process. To ensure the AFP molecular with no-specific binding of other bio-molecules, an appropriate self-assembled monolayer (SAMs) must be developed. The use of SAMs in various fields of research is growing rapidly.^{9,20–23} SAMs have been particularly applied in many biomedical fields as an interface layer between the gold electrode surface and testing solution to enhance the specific antigen-antibody interaction during the molecular recognition process.^{11,12,24}

In this study, we propose well-bonded cystamine-SAM/glutaraldehyde cross-linking layers for the immobilization of the AFP antibody. A conventional ELISA reader was used to quantitatively analyze the optical density (OD) value of the absorbed AFP antibody/antigen pairs. A commercial finite element software ANSYS was adopted to estimate the phase velocity and the mass-sensitivity of the presented FPW device. The insertion loss, operating frequency, and quality factor of the FPW transducer were investigated by a commercial network analyzer. Utilizing micro-electromechanical systems (MEMS) and cystamine-based SAM technologies, this study demonstrates a FPW-based biosensor with low insertion loss, low operating frequency, high quality factor, and sensing linearity for detecting low concentration of AFP antigen in human serum.

2 Theory Description, Simulation, and Design

2.1 Theory Description

In a FPW device, the acoustic wave propagates in a very thin plate whose thickness is much less than the wavelength. The acoustic energy is present on both sides of the plate, so the entire plate undergoes mechanical deformation. As the ratio of plate thickness to wavelength is very small, the phase velocity of the device is lower than that of most liquids, which results in no radiation from the plate to testing liquid.^{15,16} On the other hand, due to the low phase velocity, the operating frequency of the FPW device for a given wavelength is low, since

$$f_0 = \frac{V_p}{\lambda}, \quad (1)$$

where λ represents the acoustic wavelength and V_p is the phase velocity of the FPW. The mass-loading of the $\text{Si}_3\text{N}_4/\text{SiO}_2/\text{Cr}/\text{Au}/\text{ZnO}$ floating thin plate which causes changes in operating frequency is given by the following equation:

$$\frac{\Delta f}{f_0} = S_m \Delta m, \quad (2)$$

where Δf denotes the change of the operating frequency due to a change in mass per unit area (Δm) and S_m is the mass-sensitivity of the FPW device.

2.2 Propagation Properties Modeling of FPW

Based on the proposed FPW theory,¹⁵ the propagation phase velocity of FPW will be affected by the thickness of thin floating plate. In this paper, a relatively simple model of two different thin floating plates ($\text{Si}_3\text{N}_4/\text{Si}/\text{Au}/\text{ZnO}$ and $\text{Si}_3\text{N}_4/\text{SiO}_2/\text{Au}/\text{ZnO}$) has been established to investigate the influence of thickness and material of plate substrate on the phase velocity of FPW. Conventional FPW devices are constructed by $\text{Si}_3\text{N}_4/\text{Si}/\text{Au}/\text{ZnO}$ multilayer and their phase velocities are about 900 to 1000 m/s.¹⁸ To reduce the phase velocity and operating frequency of FPW, this work replaces the silicon thin plate material by silicon dioxide. The finite element model of the proposed thin floating plates is shown in Fig. 1(a). The length of the plate and the thickness of $\text{Si}_3\text{N}_4/\text{Au}/\text{ZnO}$ multilayer are set at 100 and $0.15 \mu\text{m}/0.15 \mu\text{m}/1 \mu\text{m}$, respectively. Since the thickness

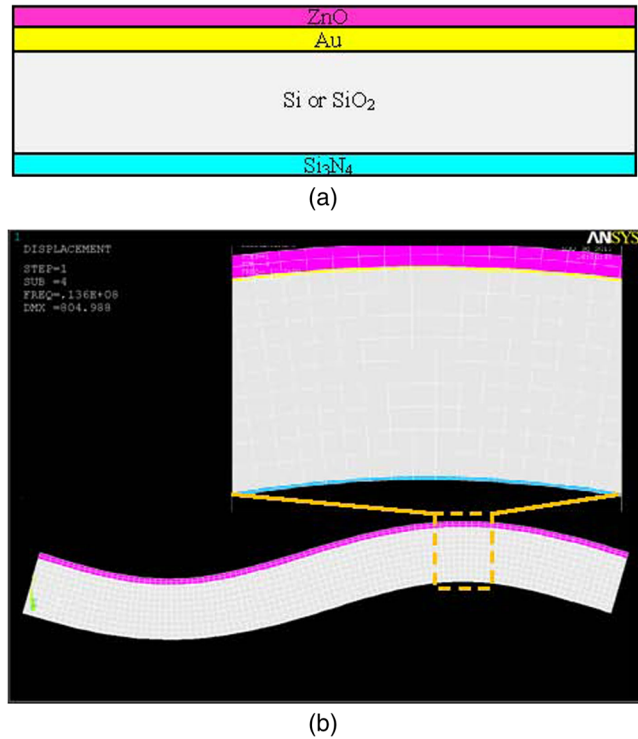


Fig. 1 (a) A simple finite element model of the proposed $\text{Si}_3\text{N}_4/\text{SiO}_2/\text{ZnO}/\text{Au}$ thin floating plate. (b) Simulated mode shape of flexural plate-wave.

of chromium ($0.02 \mu\text{m}$) is much less than that of gold electrode, it can be neglected in our simulation. The thickness of Si or SiO_2 was varied from 1 to $10 \mu\text{m}$ during the phase velocity simulation by commercial finite element software (ANSYS). All physical properties of materials adopted in this research are listed in Table 1.²⁵⁻²⁷ This simulation used two-dimensional solid structure elements that model plane strain condition in the Z direction. These elements are defined by four nodes with 2 deg of freedom. In order to obtain the Lamb wave modes, each pair of symmetric nodes from the two ends of the model was coupled. The eigenvalue problem was solved using Lanczos algorithm

Table 1 Physical properties of the materials adopted in this research.²⁴⁻²⁶

Material properties	Si	ZnO	SiO_2	Au	Si_3N_4
Young's modulus E(GPa)	190	[C] ^a	70	78	300
Density $\rho(\text{kg}/\text{m}^3)$	2330	5665	2200	19300	3100
Poisson ratio ν	0.23	—	0.2	0.44	0.27

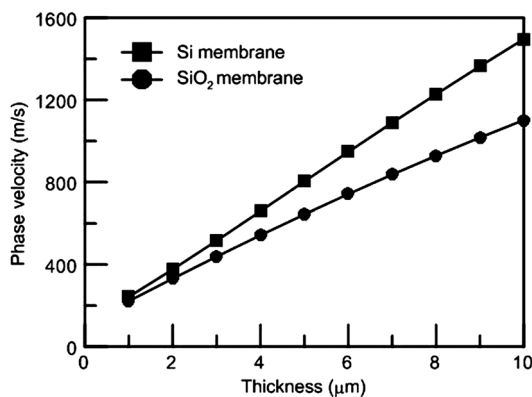
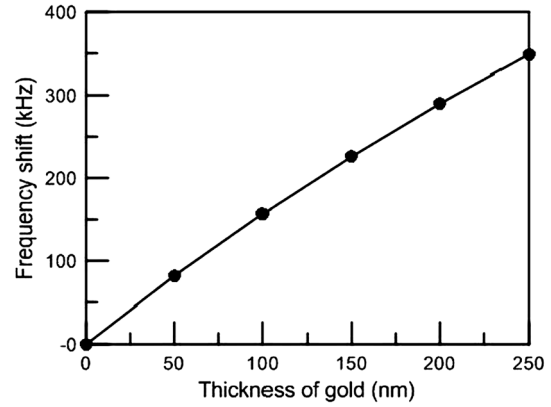
^a[C] represents the stiffness matrix of the ZnO adopted in this research,

$$[C] = \begin{bmatrix} 20.97 & 12.11 & 10.51 & 0 & 0 & 0 \\ 12.11 & 20.97 & 10.51 & 0 & 0 & 0 \\ 10.51 & 10.51 & 21.09 & 0 & 0 & 0 \\ 0 & 0 & 0 & 4.43 & 0 & 0 \\ 0 & 0 & 0 & 0 & 4.21 & 0 \\ 0 & 0 & 0 & 0 & 0 & 4.24 \end{bmatrix} \times 10^{10} \text{ N}/\text{m}^2$$

Table 2 Simulated eigenfrequencies of FPW thin floating plate with different Si(F_1) and SiO₂(F_2) thicknesses.

Thickness (μm)	F_1 (MHz)	F_2 (MHz)
1	2.43	2.219
2	3.76	3.314
3	5.16	4.385
4	6.592	5.426
5	8.034	6.436
6	9.47	7.416
7	10.89	8.365
8	12.28	9.283
9	13.642	10.169
10	14.968	11.023

for an upper frequency band of 20 MHz. This algorithm can find out all the mode shapes in the given frequency range. With these restrictions, the mode shape of the simulated A_0 mode of the Lamb wave (which also called FPW) can be obtained from a modal analysis as shown in Fig. 1(b). All the simulated eigenfrequencies with different thickness of Si and SiO₂ are shown in Table 2. It is noticeable that the length of plate shown in Fig. 1(b) is equal to one complete FPW wavelength, so the phase velocity can be calculated directly by Eq. (1) and the results are shown in Fig. 2. Obviously, the phase velocity of FPW propagated in SiO₂ is much slower than in Si under the same thickness. Consequently, in addition to low operating frequency, the operating frequency of SiO₂-based FPW is less sensitive to the thickness of thin plate and therefore it is very suitable for the development of a high stability FPW sensor. Furthermore, to analyze the mass-sensitivity of the proposed FPW device, this study simulated five different gold


Fig. 2 Simulated phase velocity of the proposed FPW device with ten different thicknesses of Si and SiO₂ thin layer.

Fig. 3 Simulated frequency shifts of the proposed FPW device under five different thicknesses of backside gold layer.

thicknesses (50 to 250 nm) deposited on the backside of a 0.15 μm Si₃N₄/5 μm SiO₂/0.15 μm Au/1 μm ZnO thin floating plate. The simulated frequency shifts under the different thicknesses of backside gold layer are shown in Fig. 3. The calculated phase velocity and mass-sensitivity of the proposed FPW device are equal to 643.7 m/s and 112 cm²/g by Eqs. (1) and (2), respectively.

2.3 Reflective Coefficient of the Proposed Groove-Type RGS

The interdigital transducer (IDT) structure is a bidirectional device and it can be converted into a unidirectional device by properly utilizing a reflector as proposed by Zaitsev and Joshi.²⁸ In this paper, we adopted groove-type RGS as the reflector of FPW and the depth of each SiO₂-groove was 1.5 μm . Nakagawa and his co-worker have presented a quantitative estimate equation of the reflection coefficient (R) of a Lamb wave with a grating reflector as shown in the following equation:²⁹

$$R = \tan h(\gamma) = \tan h\left(2 \frac{\rho_m V_{pm} - \rho_f V_{pf}}{\rho_m V_{pm} + \rho_f V_{pf}}\right). \quad (3)$$

Here, ρ_m and ρ_f are the equivalent mass densities of Si₃N₄/SiO₂/Cr/Au/ZnO floating thin plate with and without groove-type RGS, which can be calculated as 2237 and 3178.5 kg m⁻³, respectively. The V_{pm} and V_{pf} represent the phase velocity of lamb wave propagated in the Si₃N₄/SiO₂/Cr/Au/ZnO floating thin plate with and without groove-type RGS; their simulated values are equal to 429.4 and 643.7 m/s, respectively. Finally, based on Eq. (3), a 61.82% reflection coefficient of the 1.5- μm -depth groove-type RGS can be obtained.

2.4 Layout Specification of the Proposed FPW Device

Figure 4 shows a layout diagram of the designed FPW device with groove-type RGS using commercial AutoCAD software. The major design parameters of the designed FPW devices are listed in Table 3. As the width and gap of the IDT finger electrodes are 25 μm , the theoretical wavelength of FPW generated from these IDTs is equal to 100 μm (four times of IDT finger width). Both input and output IDTs of

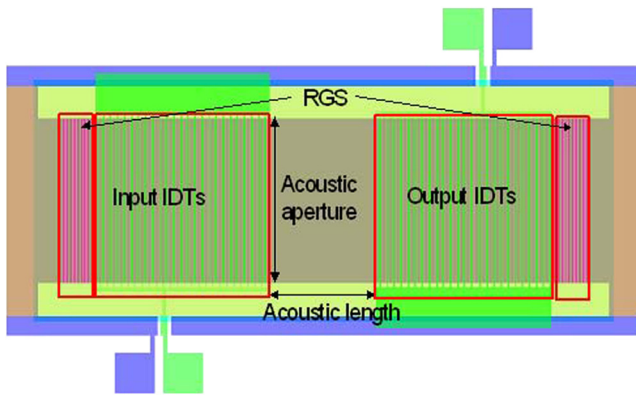


Fig. 4 Layout diagram of the presented FPW device with groove-type RGS design.

the FPW device are constructed by 25 pairs of Cr/Au fingers. The acoustic aperture and path length of the FPW devices are 2 and 1.5 mm, respectively. Each RGS of the FPW device is constructed by 3 pairs of etched grooves. The separation gap between the RGS and IDTs is 37.5 μm .

3 Experiment

3.1 Fabrication of the FPW Device

The main processing steps of the presented SiO_2 -based FPW device are shown in Fig. 5. The 5000-Å-thick silicon dioxide and the 1500-Å-thick silicon-rich low-stress nitride were grown and deposited on a 530- μm -thick 4-inch (100) silicon wafer by thermal furnace and low-pressure chemical vapor deposition system. A 5- μm -thick silicon dioxide was then deposited onto the top side by plasma enhanced chemical vapor deposition system to be the supported film for yield improvement and life time enhancement. The backside Si_3N_4 was patterned by reactive ion etching system for further backside silicon etching. As the proposed FPW devices have a conducting ground plane opposite and close to the IDTs, the transverse electric fields set up by the voltages between adjacent transducer fingers plays essentially no

Table 3 Major design specifications of the presented FPW device.

IDT finger width/gap	25 μm /25 μm
Wavelength of IDT	100 μm
Number of IDT finger pairs	25
Acoustic aperture	2 mm
Acoustic path length	1.5 mm
Number of RGS pairs	3
RGS finger width/pitch	25 μm /25 μm
Gap distance between RGS and IDT	37.5 μm

role in transduction. It is widely accepted that the (111) plane of the gold (Au) metal layers can match well with the (002) plane of ZnO layer.^{18,19,30} A 200-Å-thick Cr and a 1500-Å-thick Au were continually deposited onto $\text{Si}/\text{SiO}_2/\text{Si}_3\text{N}_4/\text{SiO}_2$ layers by an e-beam evaporator to form a ground plane of the FPW device. The Au and Cr thin layers were patterned by the Au etchant (3% I_2 : 40%KI: 57% H_2O) and the Cr etchant (Cr-7T), respectively.

Since the last decade, many piezoelectric thin films have been developed for the application of acoustic micro sensors. Three most popular piezoelectric thin-film materials are the ZnO, AlN, and PZT. In this study, a high quality C-axis orientation ZnO piezoelectric layer was deposited on the Cr/Au ground plane by RF magnetron sputter and patterned by wet etching method (3% H_3PO_4 : 3% CH_3COOH : 94% H_2O). The major advantages of magnetron sputtering are that the electron bombardment of the substrate can be greatly reduced and the temperature of substrate can be better controlled by an external heater.^{31,32} A 200-Å-thick Cr and a 1500-Å-thick Au layer was deposited by an e-beam evaporator and patterned by lift-off photolithographic method to construct the IDTs. To implement the FPW transducer with 1.5- μm -depth groove RGS, additional photolithograph and silicon etching (by reactive ion etching system) processes must be adopted, as shown in Fig. 6(f). The backside Si was etched in 30 wt%, 80°C KOH anisotropic etching solution for approximately 7 h until the whole silicon material in the backside cavity was removed. Therefore, a 0.15 μm Si_3N_4 /5 μm SiO_2 /0.02 μm Cr/0.15 μm Au/1 μm ZnO floating thin plate of the proposed FPW device can be obtained. Finally, a 0.02- μm -thick Cr and a 0.15- μm -thick Au were continually deposited on to the backside cavity for SAM immobilization.

3.2 Immobilization of the Cystamine SAM/ Glutaraldehyde Layers in the Backside Cavity of FPW Device

Molecular self-assembly is the spontaneous organization of molecules into stable, structurally well-defined aggregates. The basic principles of molecular self-assembly are found in the biology; protein folding and aggregation and pairing of base pairs in DNA are two well-known examples. SAMs were preceded historically by Langmuir–Blodgett (LB) monolayers, which have been studied extensively and are useful for many applications. LB films, however, are neither convenient to prepare nor sufficiently robust for most applications. SAMs, in contrast, are more robust and simpler to generate and can be formed from a wide variety of ligands and supports.³³ In this work, the cystamine material with amine-group bonds is adopted as a well self-assembly monolayer between the sensing gold layer and the AFP antibody layer. The detailed immobilization processes of the cystamine SAM on the FPW device are described as follows.

Before the immobilization of cystamine SAM layer, the backside gold layer surface of FPW device was pretreated with the “piranha” solution (70 wt% H_2SO_4 : 30 wt% H_2O_2) for 30 min to create a hydrophilic surface and improve the adsorption of cystamine SAM molecules and then washed with de-ionized (DI) water three times and dried at room temperature. To immobilize the SAM layer onto the gold

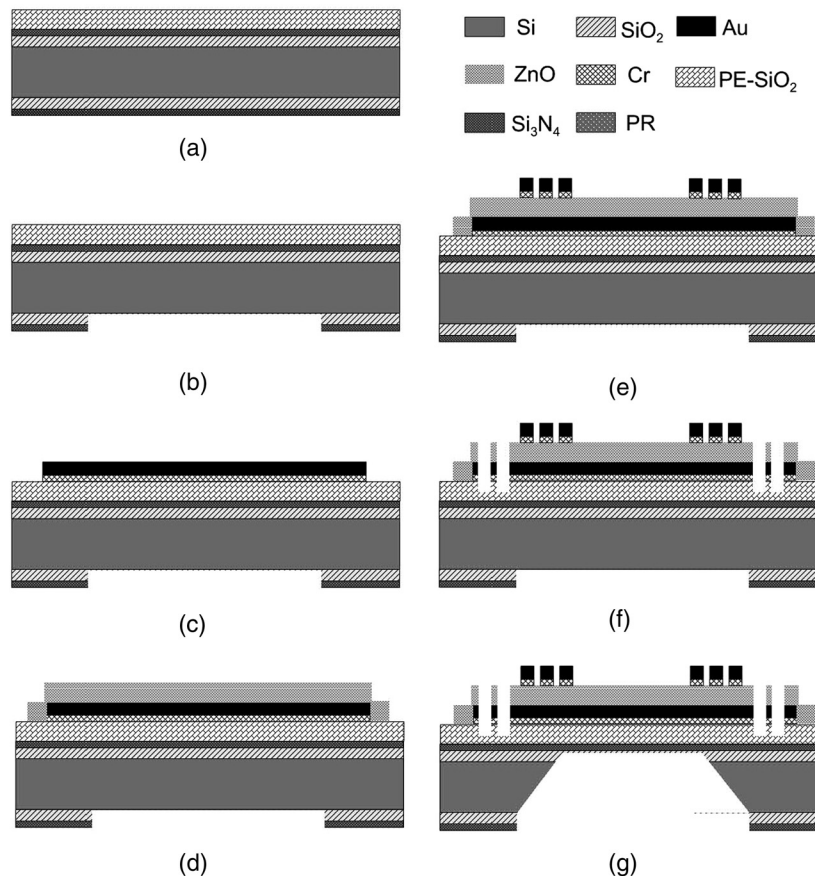


Fig. 5 Main processing steps of the proposed FPW transducer: (a) 0.5/0.15/5- μm -thick $\text{SiO}_2/\text{Si}_3\text{N}_4/\text{SiO}_2$ deposition, (b) backside Si_3N_4 patterning, (c) 0.02/0.15- μm -thick Cr/Au ground electrode deposition and patterning, (d) 1- μm -thick ZnO deposition and patterning, (e) 0.02/0.15 - μm -thick Cr/Au IDT deposition and patterning, (f) 1.5- μm -depth groove-type RGS etching, and (g) backside silicon cavity etching.

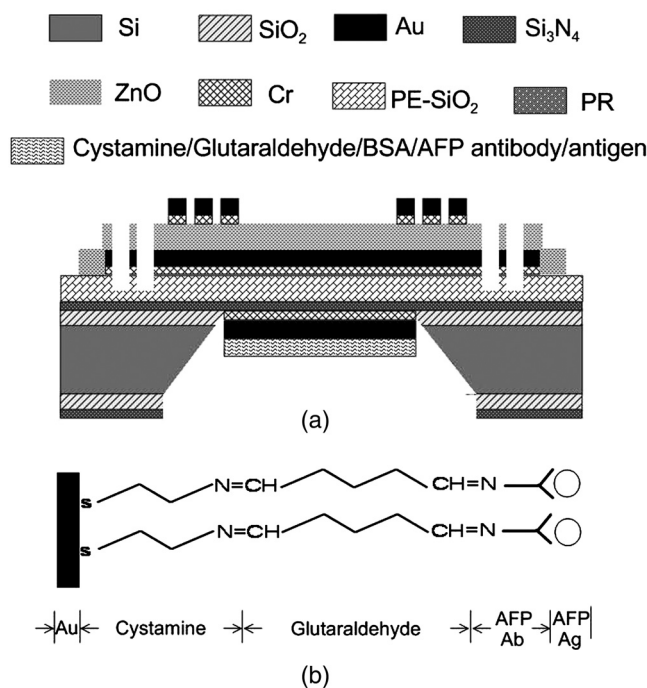


Fig. 6 (a) Final configuration of the FPW-based AFP biosensor. (b) Schematic diagram for the integration of cystamine SAM, glutaraldehyde, and AFP antibody/antigen multilayer.

layer, the chip was immersed in a cystamine solution (0.02 M) for 1 h and washed with DI water three times and air-dried. The chips were further dipped into 1.25 wt % aqueous glutaraldehyde cross-linking reagent for 1 h incubation process and washed with DI water three times.

3.3 Dip Coating of the AFP Antibody/BSA/AFP Antigen in the Backside Cavity

After the highly purified mouse anti-human AFP antibody layer coated on the surface of the backside glutaraldehyde layer, a diluted bovine serum (BSA) layer was used for blocking and incubating the AFP antibody-coated surface to avoid non-specific absorption. The final configuration of the FPW-based biosensor and the integrated cystamine SAM/glutaraldehyde/AFP antibody/AFP antigen multilayer are schematically displayed in Fig. 6(a) and 6(b), respectively. The detailed procedures are described as follows:

1. Washed by 1 c.c. phosphate buffered saline solution three times.
2. Dip 10 μL diluted rabbit AFP antibody (27°C, 2 h).
3. Inject 200 μL Tween-20 wash buffer three times.
4. Inject 10 μL , 1 wt% BSA solution (27°C, 0.5 h).
5. Inject 200 μL Tween-20 wash buffer three times.
6. Inject 10 μL diluted human AFP antigen (27°C, 2 h).

4 Results and Discussion

4.1 Quantification Analysis of the AFP Antibody-Antigen Immobilized on 96-Well Micro-Titer Plate and Si/SiO₂/Si₃N₄/Cr/Au/Cystamine/Glutaraldehyde Chip

Solid-phase assays for antibody employing ligands labeled with radioisotopes or enzymes (ELISA) are probably the most widely used of all immunological assays because many samples can be performed in a relatively short time.³⁴ In our study, a commercial ELISA was used to quantitatively analyze the total AFP concentration in a micro-titer plate and a high-linearity (99.63%) standard OD curve were extracted for six concentrations of human AFP antigen under the same monochromatic light wavelength (450 nm). A standard OD curve of the AFP antigen concentration immobilized on a Si/SiO₂/Si₃N₄/Cr/Au/cystamine/glutaraldehyde/AFP antibody chip (denoted as SAM/AFP Ab-Ag chip) with the size of 4 mm × 4 mm × 0.53 mm is also investigated. As shown in Fig. 7, the measured standard OD curve of the SAM/AFP Ab-Ag chip presents a very high linearity (99.51%), and thus, demonstrates the immobilization processes established on the silicon substrate is reliable for further developments on the FPW-based biosensor.

4.2 Characterization of the Proposed FPW-AFP Biosensor

As depicted in Fig. 8(a) and 8(b), the top-view and cross-sectional SEM of the RF sputtering deposited ZnO layer reveal its dense, uniform, and columnar grain structures. The RF sputtering deposited ZnO layer has an average grain size of about 145 nm and almost without any void. According to our previous experiences, a ZnO thin film with apparent columnar grain structures usually presents a higher C-axis (002) orientation crystallization and coupling piezoelectric coefficient. Figure 8(c) shows the top-view SEM of the patterned Cr/Au IDTs and groove-type RGS of the proposed FPW device. Each RGS of the FPW device is constructed by 3 pairs of SiO₂ etched grooves with the depth and width of 1.5 and 25 μm, respectively. The separation gap between the RGS and IDTs is 37.5 μm.

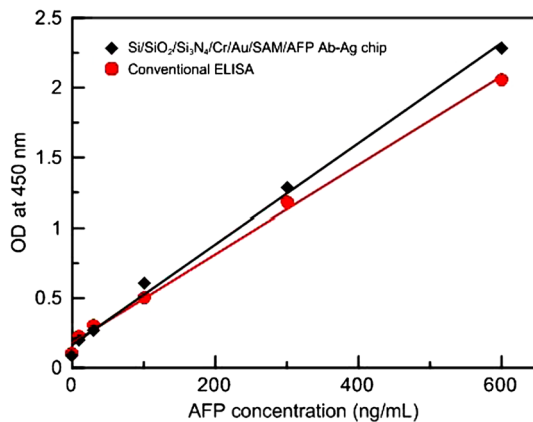
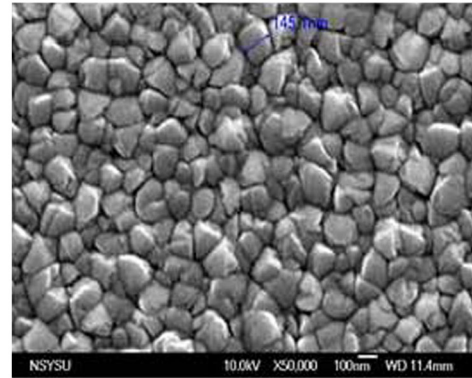
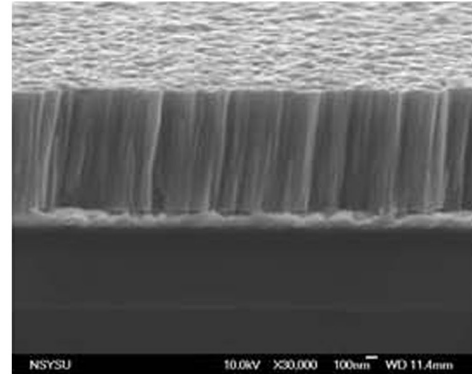


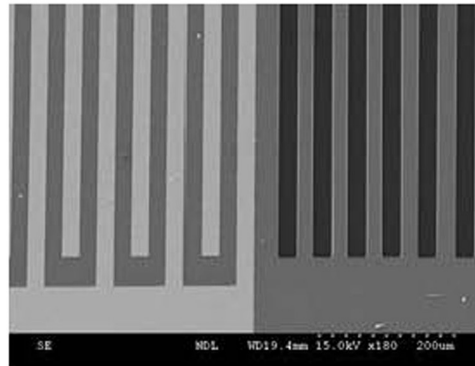
Fig. 7 The AFP standard OD curves of the 96-well microtiter plate and the Si/SiO₂/Si₃N₄/Cr/Au/cystamine/glutaraldehyde chip extracted by ELISA.



(a)



(b)



(c)

Fig. 8 (a) Top view and (b) cross-sectional SEM images of the RF sputtering deposited ZnO thin film. (c) The top-view SEM of the patterned Cr/Au IDTs and groove-type RGS of the presented SiO₂-based FPW transducer.

The center frequency of the developed FPW device was measured by the Cascade RHM-06/V probe station and the Agilent E5074 network analyzer. Two Cascade ACP40-W coplanar 150 GSG probes were used to contact the input and output IDTs of the fabricated SAW device and all the measurements were carried out at room temperature. As Fig. 9(a) shows, the measured center frequency of the implemented FPW device is 6.388 MHz, which agrees well with the simulated result (6.437 MHz). Figure 9(b) shows the frequency response measured after 0.02 μm Cr/0.15 μm Au thin films are deposited on the bottom of backside cavity of the FPW device. Obviously, as the backside Cr/Au thin films are deposited, the *Q* value of the original FPW device (206) is decreased to 148 and the center frequency of FPW shifted from 6.388 to 6.221 MHz due to

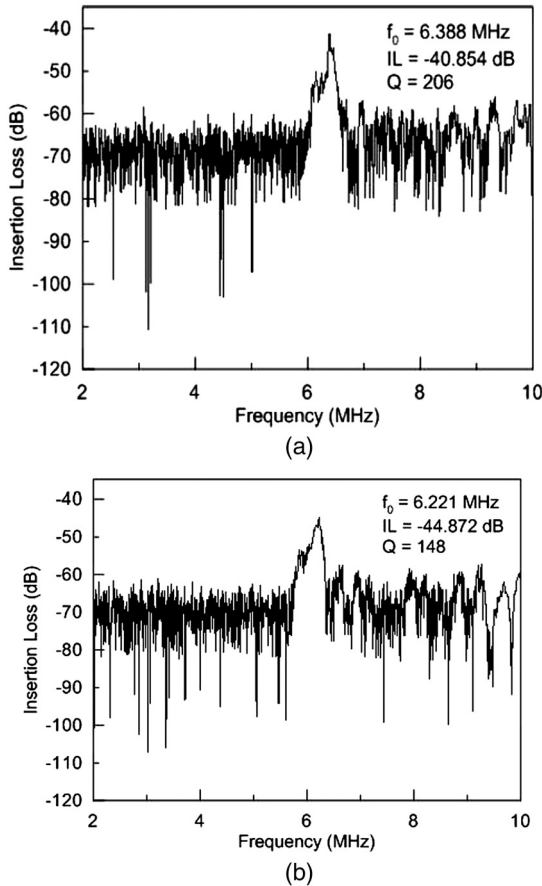


Fig. 9 Frequency responses of the proposed FPW device (a) before and (b) after the deposition of $0.02\ \mu\text{m}$ Cr/ $0.15\ \mu\text{m}$ Au thin films on the bottom of backside cavity.

the mass-loading effect. According to the theory described in Secs. 2 to 3, as the backside Cr/Au thin films are deposited, the equivalent mass densities of Cr/Au/Si₃N₄/SiO₂/Cr/Au/ZnO floating thin plate with and without groove-type RGS can be increased from 2237 to 2910.5 kg m⁻³ and increased from 3178.5 to 3553.5 kg m⁻³, respectively. The simulated phase velocity of the Lamb wave propagated in the Cr/Au/Si₃N₄/SiO₂/Cr/Au/ZnO floating thin plate with and without groove-type RGS is equal to 383.6 and 621 m/s, respectively, which is smaller than that of Si₃N₄/SiO₂/Cr/Au/ZnO floating thin plate (429.4 and 643.7 m/s). Based on Eq. (3), the reflection coefficient of the 1.5- μm -depth groove-type RGS in a Cr/Au/Si₃N₄/SiO₂/Cr/Au/ZnO floating thin plate is 57.5%, which is smaller than that of in the Si₃N₄/SiO₂/Cr/Au/ZnO floating thin plate (61.82%). It can be concluded that as 0.02- μm -thick Cr and 0.15- μm -thick Au thin films are deposited on the backside cavity, the reflection coefficient of groove-type RGS is decreased and results in a reduced Q value of FPW device.

Compared to our previous research,¹⁸ as shown in Table 4, the proposed FPW device has demonstrated a lower insertion loss (-40.854 dB), lower operating frequency (6.388 MHz), and higher quality factor (206) than conventional FPW devices with Si-based thin plate and without RGS design. Calculated by Eq. (2), the mass-sensitivity of the proposed FPW sensor is equal to 86.03 cm²/g. Finally, this research measured the center frequency shift under six various concentrations of the AFP antigen coated to the backside cavity

Table 4 A comparison of the characteristics of the proposed and conventional FPW transducer.¹⁸

	This work	Ref. 18
Center frequency (MHz)	6.388	8.751
Insertion loss (dB)	-40.854	-51.08
Quality factor	206	47.67

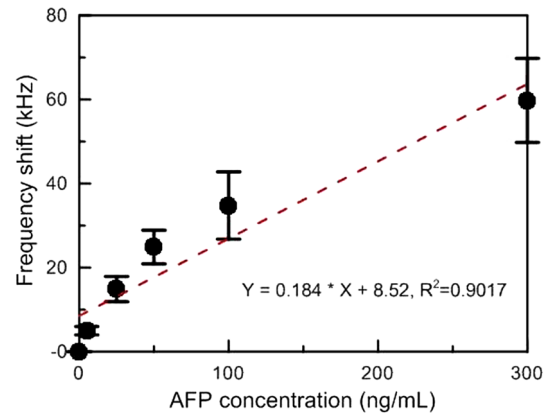


Fig. 10 Measured center frequency shift under six various concentrations of the AFP antigen coated on the backside cavity of FPW biosensor.

of FPW-based AFP biosensor and each testing condition is measured three times. As Fig. 10 shows, the proposed FPW-based AFP biosensor can demonstrate a very low detection limit of AFP antigen (5 ng/mL) and a high sensing linearity (90.7%).

5 Conclusion

In this paper, a groove-type RGS design has been adopted to improve the insertion loss and quality factor of conventional FPW-based biosensors. According to the finite element analysis results, this work also replaced silicon with silicon dioxide as the main material of FPW thin plate to reduce the operating frequency and sensitivity to thickness variation. The simulated phase velocity of the proposed FPW device constructed by Si₃N₄/SiO₂/ZnO/Cr/Au multilayer is equal to 643.7 m/s, much less than that of acoustic wave in most of testing liquid. The measured center frequency of the implemented FPW device is only 6.388 MHz, which agrees well with the simulated result (6.437 MHz) and thus can facilitate the development of readout integrated circuits. Additionally, the mass-sensitivity of proposed FPW sensor reaches 86.03 cm²/g and approximates the simulated results (112 cm²/g). By utilizing MEMS and cystamine-based SAM technologies, a novel FPW-AFP biosensor with high quality factor (206), high sensing linearity (90.7%), low insertion loss (-40.854 dB), and low detecting limit (5 ng/mL) has been demonstrated in this study.

Acknowledgments

The authors would like to thank the National Science Council and National Sun Yat-sen University of the

Republic of China, Taiwan, for financially supporting this research under Contract Nos. NSC 100-2221-E-110-021, NSC 101-2221-E-110-080, and EI-28-05-10-101. The authors are indebted to the National Nano Device Laboratories in Taiwan for their assistance in providing access to their processing facilities. The authors also thank Dr. B. S. Hsieh of Kaohsiung Medical University for her technical support in ELISA tests.

References

- C. G. Bergstrand and B. Czar, "Demonstration of a new protein fraction in serum from the human fetus," *Scand. J. Clin. Lab. Invest.* **8**(2), 174 (1956).
- S. F. Chou et al., "Determination of α -fetoprotein in human serum by a quartz crystal microbalance-based immunosensor," *Clin. Chem.* **48**(6), 913–918 (2002).
- M. H. Nguyen and E. B. Keeffe, "Screening for hepatocellular carcinoma," *J. Clin. Gastroenterol.* **35**(Suppl 2), S86–S91 (2002).
- H. M. Shingleton et al., *Gynecologic Oncology: Current Diagnosis and Treatment*, p. 604, WB Saunders, London (1996).
- E. J. Kim et al., "Immunosensing system for α -fetoprotein coupled with a disposable amperometric glucose oxidase sensor," *Sens. Actuators B* **79**(2–3), 87–91 (2001).
- T. K. Christopoulos, E. S. Lianidou, and E. P. Diamandis, "Ultrasensitive time-resolved fluorescence method for α -fetoprotein," *Clin. Chem.* **36**(8), 1497–1502 (1990).
- C. L. Morgan, D. J. Newman, and C. P. Price, "Immunosensors: technology and opportunities in laboratory medicine [Review]," *Clin. Chem.* **42**(2), 193–209 (1996).
- I.-Y. Huang, C.-Y. Lin, and E.-C. Wu, "Effects of glutaraldehyde cross-linking layer on QCM based α -fetoprotein biosensor with cystamine self-assembly monolayer," *J. Micro/Nanolith. MEM MOEMS* **9**(2), 023008 (2010).
- Y. Li, K.-S. Moon, and C. P. Wong, "Electrical property of anisotropically conductive adhesive joints modified by self-assembled monolayer (SAM)," in *Proc. IEEE Electronic Components and Technology Conf.*, Las Vegas, NV, pp. 1968–1974 (2004).
- I.-Y. Huang et al., "Development and characterization of FPW based allergy biosensor," in *Proc. IEEE International Symposium on Industrial Electronics (ISIE)*, Vigo, Spain, pp. 2736–2740 (2007).
- I.-Y. Huang, M.-C. Lee, and Y.-W. Chang, "Development of a novel flexural plate wave biosensor for immunoglobulin-E detection by using SAM and MEMS technologies," in *Proc. The 5th IEEE Conference on Sensors*, Daegu, Korea, pp. 70–73 (2006).
- X. Su, F. T. Chew, and S. F. Y. Li, "Piezoelectric quartz crystal based label-free analysis for allergy disease," *Biosens. Bioelectron.* **15**(11–12), 629–639 (2000).
- J. C. Pyun et al., "Development of a biosensor for E. coli based on a flexural plate wave (FPW) transducer," *Biosens. Bioelectron.* **13**(7–8), 839–845 (1998).
- Q. Y. Cai et al., "Vapor recognition with an integrated array of polymer-coated flexural plate wave sensors," *Sens. Actuators B* **62**(2), 121–130 (2000).
- D. S. Ballantine, Jr. et al., *Acoustic Wave Sensors: Theory, Design, and Physicochemical Application*, pp. 111–145, Academic Press, New York (1997).
- P. Luginbuhl et al., "Microfabricated Lamb wave device based on PZT sol-gel thin film for mechanical transport of solid particles and liquids," *J. Microelectromech. Syst.* **6**(4), 337–346 (1997).
- A. W. Wang et al., "A silicon-based ultrasonic immunoassay for detection of breast cancer antigens," *Sens. Actuators B* **49**(1–2), 13–21 (1998).
- I.-Y. Huang and M.-C. Lee, "Development of a FPW allergy biosensor for human detection by MEMS and cystamine-based SAM technologies," *Sens. Actuators B* **132**(1), 340–348 (2008).
- I.-Y. Huang et al., "Development of a flexural plate-wave (FPW) immunoglobulin-E allergy bio-sensing microsystem," *Sens. Actuators B* **162**(1), 184–193 (2012).
- T. Wink et al., "Self-assembled monolayers for biosensors," *Analyst* **122**(4), 43–50 (1997).
- Y. Li, K.-S. Moon, and C. P. Wong, "Formation of self assembled monolayer (SAM) on metal surfaces for high performance anisotropically conductive adhesives," in *Proc. IEEE 9th International Symposium on Advanced Packaged Materials*, Atlanta, Georgia, pp. 139–144 (2004).
- F. Pariente et al., "Enzyme support systems for biosensor application based on gold-coated nylon meshes," *Biosens. Bioelectronics* **11**(11), 1115–1128 (1996).
- D. Rhinow and N. A. Hamp, "Forming microstructured alkanethiol self-assembled monolayers on gold by laser ablation," *IEEE Trans. Nanobiosci.* **5**(3), 188–192 (2006).
- Y. Li, K.-S. Moon, and C. P. Wong, "Electrical property of anisotropically conductive adhesive joints modified by self-assembled monolayer (SAM)," in *Proc. IEEE Electronic Components and Technology Conf.*, Las Vegas, NV, pp. 1968–1974 (2004).
- J. W. Gardner, V. K. Varadan, and O. O. Awadelkarim, *Microsensors MEMS and Smart Devices*, pp. 461–462, Appendix F, John Wiley & Sons Inc., New York (2001).
- J. K. Chen, K. L. Tang, and J. T. Chang, "Effects of zinc oxide on thermal shock behavior of zinc sulfide-silicon dioxide ceramics," *Ceram. Int.* **35**(8), 2999–3004 (2009).
- T. R. Hsu, *MEMS and Microsystems: Design and Manufacture*, pp. 250–251, McGraw-Hill, Boston (2005).
- B. D. Zaitsev and S. G. Joshi, "Reflection of ultrasonic Lamb waves produced by thin conducting strips," *IEEE Trans. Ultrason. Ferroelectr. Freq. Control* **46**(6), 1539–1544 (1999).
- Y. Nakagawa, M. Momose, and S. Kakio, "Characteristics of reflection of resonators using Lamb wave on at-cut quartz," *Jpn. J. Appl. Phys.* **43**(5B), 3020–3023 (2004).
- L. Qin et al., "Analytical study of dual-mode thin film bulk acoustic resonators (FBARs) based on ZnO and AlN films with tilted c-axis orientation," *IEEE Trans. Ultrason. Ferroelectr. Freq. Control* **57**(8), 1840–1853 (2010).
- B. T. Khuri-Yakub, J. G. Smits, and T. Barbee, "Reactive magnetron sputtering of ZnO," *J. Appl. Phys.* **52**(7), 4772–4774 (1981).
- Y. Yoshino et al., "Optimization of zinc oxide thin film for surface acoustic wave filters by radio frequency sputtering," *Vacuum* **59**(2), 538–545 (2000).
- J. L. Wibur and G. M. Whiteside, *Nanotechnology*, Chap. 8, pp. 331–370, Springer, New York (1999).
- M. Steward, *Immunology*, Chapter 27, pp. 417–433, Mosby, Edingburgh (2002).



sors and biosensors.

Chang-Yu Lin received a BS degree from National Kaohsiung Normal University, Taiwan, in 2002, and an MS degree in physics from National Tsing-hua University (NTHU), Taiwan, in 2005. From 2005 to 2006, he worked at the Material Science Center of NTHU as a research assistant. He is currently working toward a PhD degree in the Department of Electrical Engineering of National Sun Yat-sen University (NSYSU). His research interests focus on acoustic sen-



I-Yu Huang received MS and PhD degrees from the Department of Electrical Engineering, National Tsing-hua University (NTHU), Taiwan. His doctoral dissertation was titled, "A monolithic high performance ISFET pH-sensor with integrated miniaturized solid-state reference electrode." During 2001 to 2002, he joined the Asia Pacific Microsystems Inc. and contributed to build up a MEMS mass-production line and the process integration of MEMS-related products. Since 2003, he has devoted his professional career as an assistant professor to the Department of Electrical Engineering, National Sun Yat-sen University (NSYSU). On February 1, 2009, he became an associate professor at NSYSU and his recent studies focus on the development of biomedical and electrochemical microsensors, electrostatic-drive microactuators, and RF-MEMS. He has been a member of the Institute of Electrical and Electronics Engineers (IEEE) since 2004. He has been director of the Operation Center of Industry and University Cooperation, NSYSU, Taiwan, since August 2010 to July 2012.



Je-Wei Lan received the BS degree from the Department of Biomedical Engineering from Chung Yuan Christian University in 2007 and MS degree in electronic engineering from Southern Taiwan University in 2010. He is currently working toward the PhD in the Department of Electrical Engineering of National Sun Yat-sen University (NSYSU), Taiwan. His research interests focus on MEMS for biomedical application.